*Korean J. Chem. Eng.*, 33(3), 735-748 (2016)
DOI: 10.1007/s11814-015-0300-y

pISSN: 0256-1115
eISSN: 1975-7220

**INVITED REVIEW PAPER**

# Environmental plasma-catalysis for the energy-efficient treatment of volatile organic compounds

**Quang Hung Trinh and Young Sun Mok†**

Department of Chemical and Biological Engineering, Jeju National University, Jeju 690-756, Korea
(*Received 24 November 2015 • accepted 30 December 2015*)

**Abstract**−Nonthermal plasma (NTP) coupled with catalysis is a promising technique for the abatement of dilute volatile organic compounds (VOCs), because it is operable under mild reaction conditions, i.e., low temperature and atmospheric pressure. This review addresses the mechanistic aspects of catalyst activation by NTP, such as the generation and fixation of reactive species, facilitation of redox cycles, photocatalysis, and local heating, to clarify the combined effects of plasma and catalysis. The plasma-catalytic removal of VOCs preferentially requires the catalyst to have a large specific surface area, high surface oxygen storage capacity, and to be highly reducible. The energy consumption and deactivation of catalysts are considered by comparing continuous and cyclic operations in terms of specific input energy, VOC removal and energy efficiencies, and byproduct formation. Based on the information in the literature, a plasma-catalytic system operating in cyclic adsorption-oxidation mode is recommended for the treatment of air contaminated by dilute VOCs. Finally, the effects of NTP on the regeneration of deactivated catalysts are also discussed.

Keywords: VOCs, Nonthermal Plasma, Catalyst, Plasma-catalysis, Cyclic Treatment, Mechanisms

## INTRODUCTION

One of the major challenges in environmental catalysis is the ability to perform the oxidation of volatile organic compounds (VOCs) at low temperatures. Compared to thermal oxidation (incineration), catalytic oxidation can largely decrease the operating temperature by lowering the activation energy barrier; however, the optimum temperature range for catalytic oxidation remains high at a few hundred degrees Celsius [1]. The most recent method for the low-temperature oxidation of VOCs is the plasma-catalyst combined process. Unlike thermal or catalytic oxidation, the plasma process operates at low temperatures, as the reaction rate is primarily determined by energy input, rather than by the reaction temperature.

Even though plasma-catalyst processes have many advantages over conventional catalytic systems, there are several problems that need to be resolved before practical implementation. Important issues surrounding the use of a plasma-catalyst may include energy consumption, formation of unwanted byproducts, catalyst preparation, and long-term stability. Addressing the issue of energy consumption more effectively requires us to pay attention to the operation mode and impedance matching between the plasma reactor and power source. Unfortunately, plasma species decompose VOCs at random, and the selectivity toward the desired product is not satisfactory. This requires unwanted byproducts other than $CO_2$ to be minimized to an acceptable level. In addition, the choice of catalytic materials and reduction method could also affect plasma-catalytic activity to a greater or lesser extent. Besides, the decomposition of VOCs using plasma may give rise to the deposition of polymer-like compounds on the catalyst, which may seriously affect the long-term stability of the catalyst. This review addresses several key aspects of plasma-catalyst combined processes such as the types of catalysts suitable for use together with plasma, plasma-mediated reduction of catalysts, catalyst activation mechanisms, energy-saving techniques through the cyclic operation of the plasma-catalytic reactor, and the in-situ regeneration of deactivated catalyst using plasma.

†To whom correspondence should be addressed.
E-mail: smokie@jejunu.ac.kr


## PLASMA-CATALYTIC REACTOR SYSTEMS FOR ENVIRONMENTAL APPLICATIONS

### 1. Principle of Dielectric Barrier Discharge

Non-thermal plasma (NTP) or partially ionized gas consisting of various species such as energetic electrons, ions, radicals, excited molecules and atoms, and neutral molecules is characterized by its thermal non-equilibrium state, in which the temperature of electrons (1-10 eV) is much higher than that of ions and neutral species [2,3]. Dielectric barrier discharge (DBD) is an easily available method commonly used to generate NTP at atmospheric pressure. Typical arrangements of a DBD plasma generator are shown in Fig. 1. At least one insulating layer is present in the gap between the high voltage and ground electrodes as a dielectric barrier [4].

Numerous microdischarges occur when the voltage across the gas gap exceeds the gas breakdown voltage, featured by processes of electron multiplication, excitation, dissociation, ionization, and space charge accumulation. The presence of dielectric layers limits the amount of charge and energy imparted to an individual microdischarge, thereby distributing the microdischarges over the entire electrode area. Unlike corona discharge, DBD is destined for applications of large volume plasma chemistry such as ozone genera-

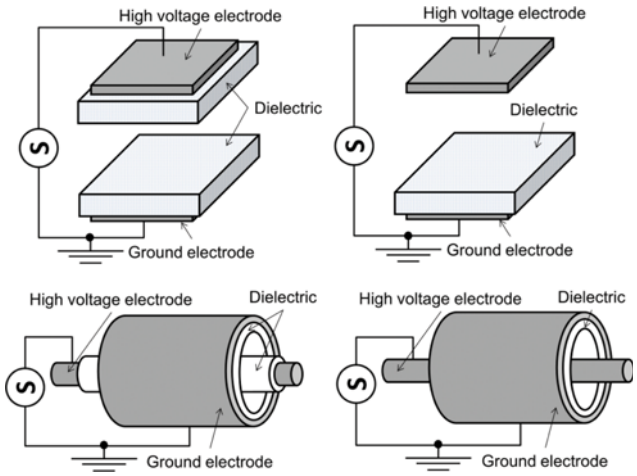


**Fig. 1. Arrangement of typical DBD plasma reactors.**

tion, surface treatment, and air pollution control [4,5].

**2. Plasma-catalytic Reactor Systems for Environmental Applications**

To date, various designs of plasma-catalytic reactors have been studied. Generally, there are two types of combined plasma-catalyst processes, i.e., catalyst-in-plasma and catalyst in post-plasma, also known as one-stage and two-stage configurations, respectively. Obviously, catalyst-in-plasma is more effective in most environmental application cases, because the catalyst is in direct contact with the plasma and air contaminants entering the reactor for oxidation to carbon dioxide and water vapor by plasma-activated catalysis. Catalysts intended for combination with plasma can be either pellets or monolithic [6-9]. In general, a packed-bed reactor provides more effective contact between the reactant and catalyst than other types of reactors, but the pressure drop across the reactor is necessarily high. The merit of monolithic reactors is the low pressure drop across the reactor [10]; however, the contact between the reactant and catalyst surface is often less than desirable. Clearly, there is a tradeoff between the merits and demerits for each type of reactor.

**3. Power Measurement Using Lissajous Q-V Figure**

One of the most important aspects when considering plasma for environmental application is the energy consumption. The energy consumed by a DBD plasma reactor during one voltage cycle is commonly determined as the area of a Lissajous figure that shows the flowing charge Q as a function of the applied voltage V [11]. The equivalent electrical circuit for an unpacked DBD reactor is shown in Fig. 2(a). Without plasma discharges, the reactor merely consists of a capacitance series of $C_G$ and $C_D$. As the plasma discharge is triggered, the resistance of gas gap $R_G$ is taken into account. In the majority of DBD applications, the shape of the Lissajous figure is close to that of an ideal parallelogram [5], in which the BC and DA sides with a slope of $dQ/dV=C_D$ correspond to two discharge periods during a voltage cycle (Fig. 2(b)). The average power dissipated during discharge can be calculated by multiplying the area with the frequency or using Manley's equation [12,13]:

$$P = 4fC_D V_o \left( V_{peak} - \frac{C_G + C_D}{C_D} V_o \right), \quad (1)$$

where f, $V_o$, and $V_{peak}$ are the frequency, onset, and peak values of the applied voltage, respectively.

For a packed-bed reactor, the discharge power can be calculated by using a Lissajous V-Q figure in the same way as with the unpacked reactor. However, the use of Manley's equation requires addition of the capacitance of the packing layer. Thus, according to Eid et al. [14], the calculation is facilitated by replacing the packing material with an equivalent dielectric material with the same dielectric constant and filling a region near the high voltage (HV) electrode, as shown in Fig. 3(a). This equivalent region of packing material is calculated based on the total weight of the packing material and its density. The electrical circuit without plasma turns into a series of $C_D$ and the equivalent capacitances of packing material $C_P$ and gas gap $C_G$ (Fig. 3(b)). In principle, these capacitances are calculated as follows:

$$C_P = \frac{2\pi\varepsilon_o\varepsilon_{rp}L}{\ln(R_P/R_E)}, \quad (2)$$

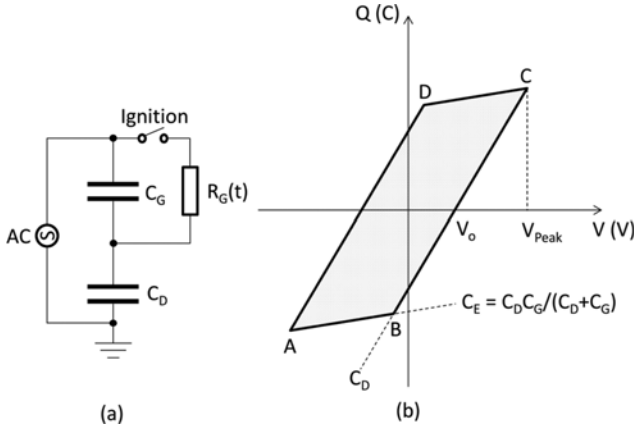


**Fig. 2. Equivalent electrical circuit and Lissajous figure of an unpacked DBD plasma reactor ($C_D$: capacitance of dielectric, $C_G$: capacitance of gas gap and $C_E$: equivalent capacitance of $C_D$ and $C_G$ connected in series).**

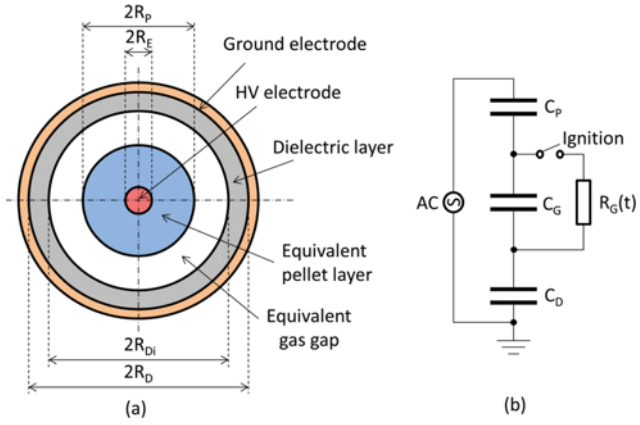


**Fig. 3. Equivalent model and electrical circuit of a packed-bed reactor.**

$$C_G = \frac{2\pi\varepsilon_o L}{\ln(R_{Di}/R_P)}, \quad (3)$$

$$C_D = \frac{2\pi\varepsilon_o\varepsilon_{rd} L}{\ln(R_D/R_{Di})}, \quad (4)$$

where $\varepsilon_o$ is the permittivity of free space ($8.854\times10^{-12}$ F m$^{-1}$), $\varepsilon_{rp}$ is the relative permittivity of packing material, $\varepsilon_{rd}$ is the relative permittivity of the dielectric, and L is the active length of the reactor.

**4. Generation of Reactive Species**

In NTP generation by electrical discharge, substantial part of the electrical energy input is spent to energize electrons rather than to heat the entire bulk gas. The hot (or energetic) electrons can trigger many chemical processes such as dissociation, excitation, and ionization of molecules. As a consequence, various reactive species such as OH, O, and N radicals; excited $N_2$ and $O^+$ and $O_2^+$ ions are formed [15]. Their highly reactive properties enable these species to rapidly recombine or react with bulk gas molecules. The recombination of radical and neutral species can also lead to the formation of some additional radical species and reactive molecules (e.g., $O_3$, $HO_2$, and $H_2O_2$) [16].

## PLASMA-CATALYSIS MECHANISMS

Generally speaking, catalyst activation refers to the breaking of a chemical bond on the catalyst surface. In the presence of plasma, a catalyst can be activated in various ways; hence, we cannot explain plasma-catalysis with one or two mechanisms. As many researchers have reported, plasma-catalysis provides an alternative reaction pathway with lower activation energy. In a plasma-catalytic system, the activation energy can be provided by fast electrons, radicals, photons, and heat, and which of these mechanisms is dominant will depend on the type of catalyst, reactants, reaction condition, etc.

**1. Generation of Surface Oxygen Atom**

In thermal catalysis, the dissociative adsorption of oxygen occurring at high temperature can explain the generation of active oxygen on the surface. In fact, many catalytic oxidation reactions begin with the generation of active oxygen in this way. On the other hand, the exposure of a catalyst to plasma results in the highly reactive species generated by the plasma, such as fast electrons and radicals, to break the oxygen bond to produce active oxygen. It has been stated that electron-assisted surface processes, including electron-induced dissociation of adsorbed oxygen molecules, create the majority of the oxygen ions involved in the formation of an oxide on a metal surface immersed and floating in oxygen plasma [17]. In the presence of a catalyst, the electric field close to its surface is enhanced compared to the field in the stream channels, thereby leading to an enhanced production of O atoms. Those O atoms involved in surface reactions, due to their short lifetime, are required to be produced on or near the surface of the catalyst [18,19].

**2. Fixation of Reactive Species on the Surface**

Extension of the lifetime of reactive species generated in the plasma gas phase by adsorption on the surface can promote oxidation reactions. In the gas phase, the lifetime of reactive species such as O and OH radicals is extremely short because of rapid recombination, and not all the oxidative radicals generated by plasma are used for VOC decomposition. In comparison, when O and OH formed in the gas phase are adsorbed on the surface, their effective lifetimes substantially increase. In this sense, the removal of VOC would be expected to be more effective on the surface than in the gas phase.

Guaitella et al. investigated atomic adsorption on $TiO_2$ and $SiO_2$ particles exposed to plasma and found that the plasma-induced oxygen atoms that were grafted to the oxide surface remained long after plasma exposure. These bounded O atoms were able to oxidize $C_2H_2$ under normal conditions without exposure to plasma or UV light [20]. The deposition of O atoms on a Pyrex discharge tube pretreated by RF plasma was also confirmed via monitoring the transformation of NO to $NO_2$ in a post-plasma experiment [21]. The surface density of atomic oxygen on the Pyrex surface was estimated to be ca. $2\times10^{14}$ cm$^{-2}$ at an injected power of 30 W under low-pressure conditions (0.53 mbar). Separately, Kim et al. [22] experimentally studied the plasma-induced fixation of gas-phase oxygen on the surface of several catalysts at atmospheric pressure using isotopically labeled molecular oxygen ($^{18}O_2$). It was found that NTP is able to fix oxygen species onto the surface of the catalyst. The adsorbed $^{18}O$-labeled oxygen species were found capable of surviving for a certain period of time (about 30 min), and are easily activated by subsequent plasma discharge for participation in oxidation reactions. The existence of both adsorbed atomic and molecular oxygen on a $MnO_x$ catalyst immersed in DBD plasma was reported by Guo et al. [23] using X-ray photoelectron spectroscopy (XPS). The binding energies (BE) assigned to adsorbed O and $O_2$ were 531.0±0.5 and 532.6±0.5 eV, respectively.

Investigation of the NTP regeneration of isopropyl alcohol (IPA) saturated titania ($TiO_2$) under the influence of humidity led Sivachandiran et al. [24] to observe that the mineralization and carbon balance were greatly improved by increasing the air relative humidity (RH). According to the authors, OH radicals generated by humid air plasma became chemisorbed onto $TiO_2$, leading to re-hydroxylation of the $TiO_2$ surface and, consequently, the oxidation of adsorbed IPA. Similar behavior in $CO_2$ selectivity and material balance was reported by Zhu et al. [25] who studied the continuous plasma-catalytic decomposition of acetone ($CH_3CO$-$CH_3$). However, there is an optimum level of RH (10% in Ref. [25] and 20% in Ref. [26]) for VOC decomposition efficiency, since high RH inhibits the formation of energetic electrons because of water adsorbing onto the catalyst and blocking active sites. Quantities of OH radicals in the plasma gas phase and catalyst surface can be estimated by using salicylic acid (SAL) as an OH scavenger [23,27]. It was reported that, at a specific input energy (SIE) of 62.5 Wh m$^{-3}$ or 225 J L$^{-1}$, the amount of gaseous OH radicals in the presence of $MnO_x/Al_2O_3$/Nickel foam was much less than that in the absence of the catalyst, namely $17.04\times10^{13}$ cm$^{-3}$ and $111.38\times10^{13}$ cm$^{-3}$, respectively [23]. A large portion of OH radicals evaluated to be $89.14\times10^{13}$ cm$^{-3}$ were found to adsorb on the catalyst surface and to be responsible for the enhanced VOC removal efficiency.

The adsorption of reactive species as well as VOCs on a catalyst generally depends on the nature of its surface and its porosity. The effect of catalyst porosity on the plasma-catalytic oxidation of

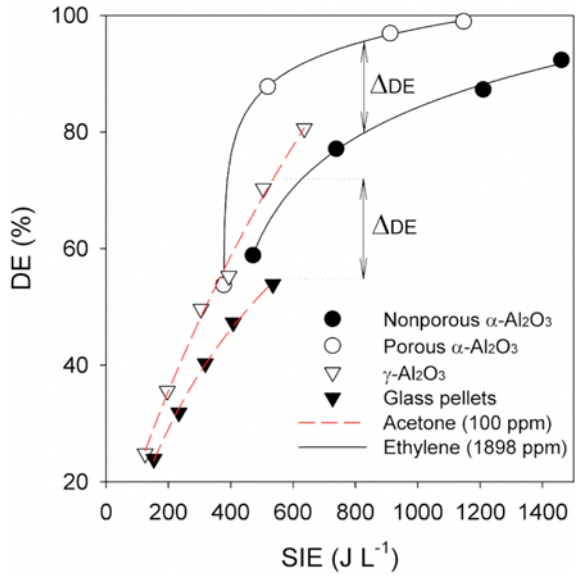


**Fig. 4. Effects of catalyst porosity on decomposition efficiencies of ethylene [28] and acetone [29].**

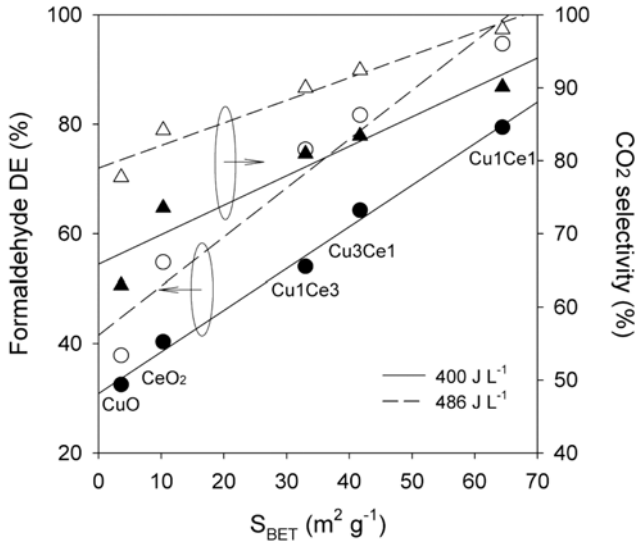


**Fig. 5. Formaldehyde (57.7 ppm) decomposition efficiency and $CO_2$ selectivity as functions of BET surface area at an SIE of 400 J $L^{-1}$ (data extracted from the figures given in Ref. [30]).**

ethylene ($C_2H_4$) and acetone was examined by Gandhi et al. [28] and Zheng et al. [29]. Their experiments clearly showed that the introduction of an adsorbent into plasma discharge largely improved the VOC decomposition efficiency (DE). As seen from Fig. 4, the introduction of porous alumina with a large surface area decomposed more VOCs than the cases of non-porous materials, such as glass and non-porous alumina, due to the extension of the lifetime of reactive species by adsorption. Moreover, the use of porous alumina could successfully avoid the formation of partially oxidized byproducts (e.g., acetaldehyde and formaldehyde), as well as minimize the emission of ozone and nitrogen oxides. Similar to reactive species, VOC molecules can also be fixed onto the surface. In the gas phase, molecules have random motions; on the other hand, a molecule adsorbed on the surface vibrates at a fixed position and is more likely to be attacked by the reactive species [28]. Zhu et el. [30] investigated the oxidation of formaldehyde (HCHO) by plasma catalysis over a series of Cu-Ce oxides (with different Cu/Ce ratios) and found that the specific surface area ($S_{BET}$) and pore volume of catalysts followed the same order as the HCHO decomposition efficiency and $CO_2$ selectivity (percentage ratio of $CO_2$ to total amount of CO and $CO_2$): Cu1Ce1>Cu3Ce1>Cu1Ce3>$CeO_2$>CuO. By extracting data from the figures given in Ref. [30] at a certain SIE, the above catalytic performances are found to almost linearly increase with increasing $S_{BET}$ (Fig. 5). This implies that adsorption is a crucial step in plasma catalysis. As pointed out by Kim et al. [31], surface reactions dominate the plasma-catalytic decomposition of VOCs, which follows zero-order kinetics. In fact, not only the textural properties but also other factors such as the surface chemistry and morphology of a catalyst also influence its activity, especially toward $CO_2$ selectivity. These aspects will be discussed in the subsequent sections.

Beside the above short-lived species, ozone also plays an important role in the low-temperature activation of catalysts. In the presence of oxygen, plasma discharge necessarily produces ozone. Ozone can readily be destroyed on the catalyst ($MnO_2$, CuO, Ag, etc.) to generate the more reactive oxygen atom [32-35]. Note that the oxidation potential of atomic oxygen is far higher than that of ozone. The surface decomposition of ozone into atomic oxygen on a manganese oxide catalyst has been well established by Li et al. [36]. As proposed by the authors, the process is initiated by the dissociative adsorption of ozone on the catalyst surface, generating adsorbed oxygen atoms, which in turn react with gaseous ozone to form diatomic oxygen. The mechanism is summarized as follows:

$$O_3+*\rightarrow O_2+O* \quad (5)$$

$$O_3+O*\rightarrow O_2+O_2* \quad (6)$$

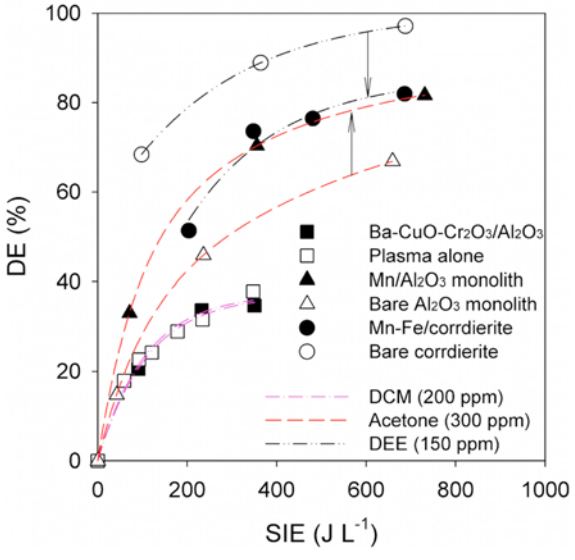


**Fig. 6. Effects of ozone decomposition catalysts on decomposition of different VOCs in one-stage reactor (data given in Ref. [44], [45] and [48] for DCM, DEE and acetone, respectively).**

$$O_2^* \rightarrow O_2 + * \quad (7)$$

where the * symbol represents an active site. Many researchers have reported the synergistic effects of plasma and ozone decomposition on catalyst combination, especially in post-plasma configuration [37-43]. However, the direct exposure of an ozone decomposition catalyst to plasma is not recommended in terms of VOC removal efficiency in the case of various VOCs such as dichloromethane (DCM), diethyl ether (DEE) and ethylene [44-46]. As shown in Fig. 6, the introduction of a Ba-CuO-$Cr_2O_3$/$Al_2O_3$ catalyst for destroying ozone in plasma did not lead to the enhanced decomposition of DCM compared to plasma alone. Even worse, in the presence of cordierite supported Mn-Fe mixed oxide, the decomposition efficiency of DEE substantially decreased compared to that of bare cordierite, which did not display any catalytic activity toward ozone destruction. Presumably, under plasma conditions, a portion of $O_3$ produced on or in the vicinity of the catalysts is rapidly decomposed catalytically to $O_2$ without any contribution to VOC oxidation. Nevertheless, this enhancement effect for ozone decomposition catalysts was often observed for acetone decomposition in a one-stage reactor [25,47,48]. Unlike acetone, though, the former VOCs are more reactive even with gaseous ozone. There is a trade-off between the amount of atomic oxygen produced from ozone decomposition and that of ozone formed for directly oxidizing VOCs. Selecting an appropriate catalyst and reactor configuration is therefore important for achieving high VOC removal efficiency.

Although the diffusion and stabilization of short-lived species as well as the ignition of plasma within catalyst micropores are not well understood, the extent to which ozone is able to access the pores apparently affects the reaction performance. Huang et al. [49] investigated the removal of toluene by plasma-driven catalysis using various types of zeolites at atmospheric pressure and room temperature. Their experimental results showed that carbon balance and $CO_2$ selectivity followed the same order of pore size, HY> H$\beta$>HZSM-5>5A, which was opposite to the ozone emission. The toluene removal efficiency was observed to be slightly different in the following the order: H$\beta$>HY>HZSM-5>5A. Among the catalysts used, 5A zeolite had the smallest pore diameter of about 5 Å, which is insufficient for the diffusion of ozone (5.8 Å) and toluene (5.85 Å). Meanwhile, other zeolites with larger pore sizes allowed additional reactants to access the micropores and subsequently react on the internal surfaces. Silver loaded onto HY zeolite accelerated ozone decomposition, acting as O reservoir for the deep oxidation of toluene.

**3. Facilitation of Redox Cycle**

A transition metal oxide catalyst repeats its oxidation and reduction in cycles. In traditional thermal catalysis, molecular oxygen is involved in the re-oxidation of the catalyst in the redox cycle. In comparison, under plasma discharge, highly reactive O atoms are also involved in the re-oxidation, leading to an enhanced oxidation capability. Yamamoto et al. [50] investigated the influence of different transition metal oxides on the plasma oxidation of diesel particulate matter (PM). Four metal oxides ($TiO_2$, ZnO, $V_2O_5$, and especially $Fe_2O_3$) have positive catalytic oxidation rates under plasma discharge, whereas $MnO_2$, $Co_3O_4$, and CuO show negative catalytic oxidation rates compared to that of plasma alone (Fig. 7). It is generally recognized that the formation enthalpy of metal oxide (per mole of oxygen atoms) is a measure of the oxidation activity of a metal oxide catalyst. A transition metal oxide with an appropriate formation enthalpy exhibits high oxidation activity because it is more likely to release oxygen atoms bound to metal atoms. If the formation enthalpy is too high or too low, the redox catalytic cycle does not readily occur, and the oxidative catalytic activity of such a transition metal oxide is low. When a plasma-catalytic process based on the use of a metal oxide was applied to the decomposition of IPA [51], iron oxide also performed well, similar to the case of diesel PM oxidation. In the absence of a metal oxide catalyst, the decomposition of IPA produced $CO_2$, CO, and acetone in almost equal amounts together with several other partially oxidized byproducts. Even if the use of CuO largely increased $CO_2$ selectivity, substantial amounts of CO and acetone were still retained. However, in the presence of an iron oxide catalyst, acetone, CO, and other partially oxidized byproducts totally disappeared, leaving only $CO_2$ as the byproduct. Similar results were recently reported by Guo et al. for the plasma-catalytic decomposition of toluene using various transition metal oxides: CuO, $CoO_x$, $FeO_x$ and $MnO_x$ [52]. Among these catalysts, $FeO_x$ showed a relatively high catalytic activity toward toluene conversion and $CO_2$ selectivity, especially at low energy injections.

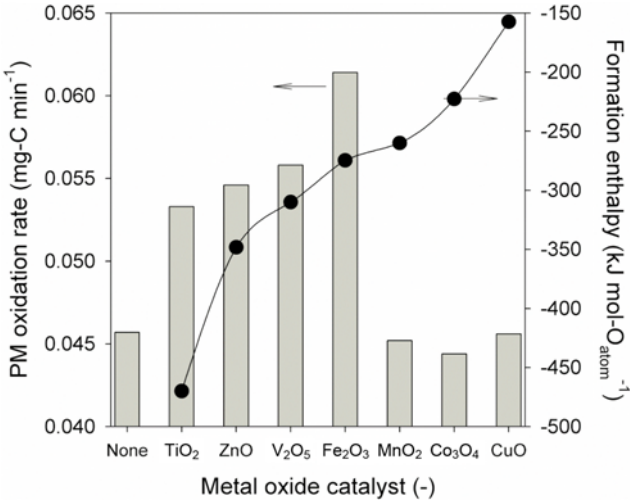


**Fig. 7. PM oxidation rate and formation enthalpies of metal oxide catalysts (discharge power: 1.0 W, gas flow rate (10% $O_2$ with $N_2$ balance): 0.5 L $min^{-1}$, reactor temperature: 200 °C, data extracted from Ref. [50]).**

In general, the abundance and mobility of surface oxygen have been found to govern the performance of catalytic oxidation reactions. The virtue of a supported metal oxide depends not only on the formation enthalpy but also on the interaction between the active component and support, as well as on the catalyst dispersion. By using X-ray diffraction (XRD) and temperature programmed reduction (TPR), Zhu et al. [47] confirmed that for various $Al_2O_3$ supported metal oxides, including $CeO_2$, $Co_3O_4$, CuO, $MnO_2$, and NiO (denoted as $MO_x/\gamma$-$Al_2O_3$), the amount of $H_2$ consumed and therefore the amount of surface oxygen followed a reverse trend as compared to the crystalline size, as seen in Fig. 8. The catalyst reduc-

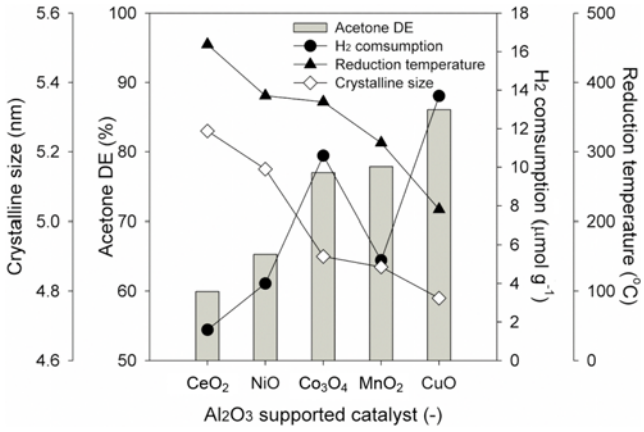


**Fig. 8. Acetone decomposition efficiency, amount of $H_2$ consumed, reduction temperature, and crystalline size as functions of the alumina-supported catalyst used (SIE: 900 J $L^{-1}$, acetone initial concentration: 1,184 ppm, total gas flow rate: 1.0 L $min^{-1}$, data given in Ref. [47]).**

ibility in terms of lowest reduction peak temperature, instead, decreased with crystalline size. Although $MnO_2$ possesses a high formation enthalpy per mole of O atoms (absolute value) and a similar crystalline size compared to those of $Co_3O_4$, the lower reduction temperature and $H_2$ consumption of $MnO_2$ were attributed to the effect of metal-support interaction. The catalytic activity towards acetone decomposition efficiency over $MO_x/\gamma$-$Al_2O_3$ under DBD plasma activation clearly reflected the reducibility and surface oxygen storage properties, with $CuO/\gamma$-$Al_2O_3$ being the most active catalyst.

The facilitation of redox cycles by NTP under mild conditions contributes to synergistic effects of plasma catalysis on both conversion and selectivity. Ding et al. [53] reported that 99% of 276 ppm HCHO in an air stream can be effectively destroyed ($P_{HCHO\ to\ COx}$, as shown in Fig. 9) on a $Ag/CeO_2$ catalyst at a reaction temperature and SIE of 70 °C and 108 J $L^{-1}$, respectively. This HCHO conversion was higher than the simple sum of those from individual thermal and plasma effects (33% on $Ag/CeO_2$ without plasma and 57% on fused silica with plasma). In this regard it is noteworthy that the conversion obtained on fused silica was considered as the pure plasma-induced conversion, because the specific surface area of fused silica pellets is nearly zero (<<0.1 $m^2$ $g^{-1}$). Yet, the plasma-catalyst combined effect was even more profound on the degree of $CO_2$ formation ($P_{HCHO\ to\ CO_2}$), which resulted from the subsequent oxidation of CO to $CO_2$ and/or alteration of the HCHO destruction pathway. The former was confirmed by CO oxidation experiments under the same conditions (see Fig. 9). According to the authors, the synergistic effects between the DBD plasma and $Ag/CeO_2$ catalyst can be well explained by the plasma-assisted catalytic redox cycles including Ag-$Ag_2O$ and $Ce_2O_3$-$CeO_2$ inter-conversions. The plasma-generated O and $HO_2$ radicals play necessary roles in re-initiating these redox cycles at low temperatures.

Unlike in conventional catalysis, surface OH groups as well as adsorbed and even lattice oxygen can be activated by NTP at low temperatures. Involvement of these species is evidenced by the formation of nitrogen and carbon oxides in plasma in the absence of oxygen and water vapor [54-56]. Fig. 10 shows the concentrations of $N_2O$ and $CO_x$ formed by $N_2$ plasma activation of $BaTiO_3$ and $FeO_x$/SBA-15 catalysts, respectively. As seen, the content of all produced oxides follows similar decreasing trends within certain periods

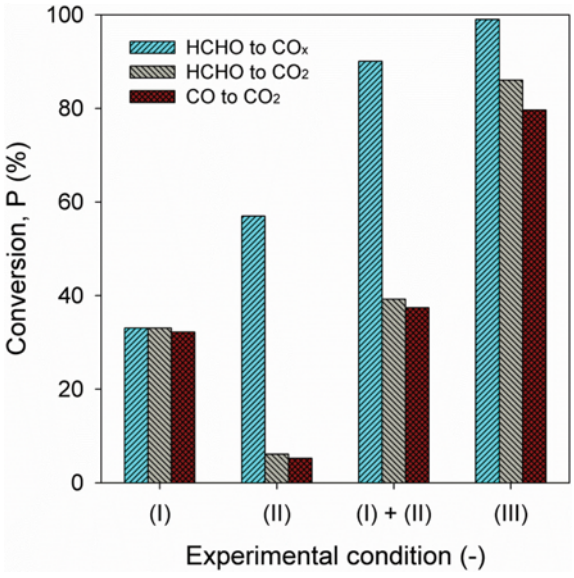


**Fig. 9. Conversions of HCHO and CO on $Ag/CeO_2$ and fused silica at 70 °C ((I): $Ag/CeO_2$ without plasma, (II): fused silica with plasma, (I)+(II): simple sum of conversions obtained under (I) and (II) conditions and (III): $Ag/CeO_2$ with plasma; SIE: 108 J $L^{-1}$, HCHO: 276 ppm, CO: 200 ppm and $H_2O$: 1.0% in air, data given in Ref. [53]).**

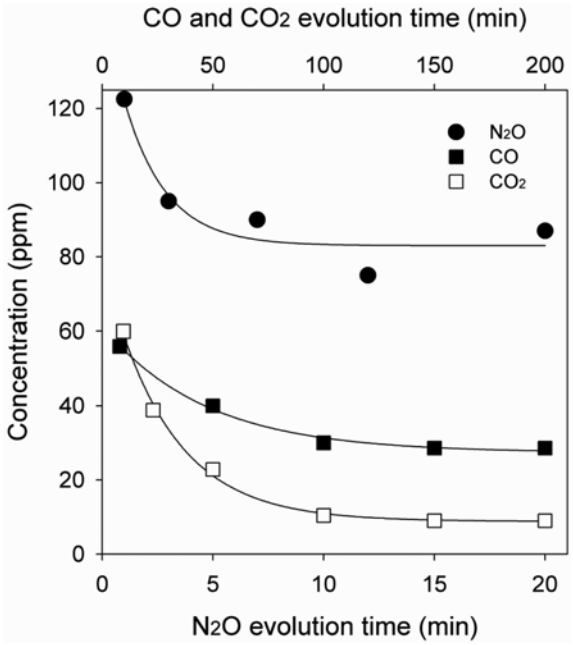


**Fig. 10. $N_2O$ formation in a $BaTiO_3$ packed-bed reactor with dry $N_2$ plasma (applied voltage: 7.0 kV) [54] and $CO_x$ ($x$=1 *or* 2) formation in a DBD $FeO_x$/SBA-15 packed-bed reactor with dry toluene-containing $N_2$ plasma (initial toluene concentration: 100 ppm, SIE: 284 J $L^{-1}$) [55].**

and remains unchanged thereafter for long times. The observations suggest that the oxygen atoms on the catalyst surfaces were initially consumed, and at stationary states, even lattice oxygen atoms were involved in reactions. $O_2$-containing plasma is able to compensate the transferred surface oxygen by generating O atoms and therefore promote the redox catalytic cycles. By using XPS, Zhu et al. [30] observed a perfect correlation between reaction performance and oxygen storage capacity in terms of adsorbed oxygen ($O_{ads}$) concentration (i.e., the ratio between adsorbed oxygen and total adsorbed and lattice oxygen) of Cu-Ce oxide catalysts for the plasma-catalytic removal of formaldehyde. The highest $O_{ads}$ concentration and best performance were achieved over a Cu1Ce1 catalyst (shown in Fig. 5).

**4. Plasma-induced Photocatalysis**

Another reactive species generated by plasma are photons. The most abundant component in contaminated air is nitrogen. Electrical discharge in nitrogen generates weak ultraviolet (UV) light with various wavelengths in the range of 300-400 nm. Basically, in this wavelength range UV light alone does not promote the decomposition of VOCs. However, this UV light can initiate photocatalytic reactions, which are intrinsically very slow, which is why the effect of photocatalysis is not remarkable, compared to thermal catalysis based on metals or metal oxides. Moreover, the UV energy emitted from plasma is usually small compared to the electrical input energy [57]. According to Sano et al. [58], the energy of UV illumination generated from a cylindrical type surface discharge reactor was measured to be 2.5 μW $cm^{-2}$ (air plasma, frequency: 24 kHz and input power: 5 W), which is far lower than that of conventional photocatalysis [59]. However, more recently, Pekárek et al. [60] reported that plate-type surface dielectric barrier discharge for ozone generation produced much higher UV energy with ca. 3,000 μW $cm^{-2}$ (air plasma, wavelength: 365 nm, discharge power: ca. 5.5 W and frequency: 10.9 kHz). As a result, the presence of a photocatalyst such as $TiO_2$ and ZnO in the discharge chamber enhanced ozone production. The reason for the large discrepancy in UV emission under similar conditions is not clear.

Gandhi et al. demonstrated that plasma-photocatalytic activity is shape-dependent [61]. In their work, three different ZnO photocatalysts, namely nanoparticles (NPs), nanorods (NRs), and nanowires (NWs) were prepared, and then loaded onto monolithic porous alumina ceramic. The presence of ZnO slightly increased the butane decomposition due to the photocatalytic effect, but regardless of the shape of ZnO, all the three ZnO photocatalysts exhibited simi-

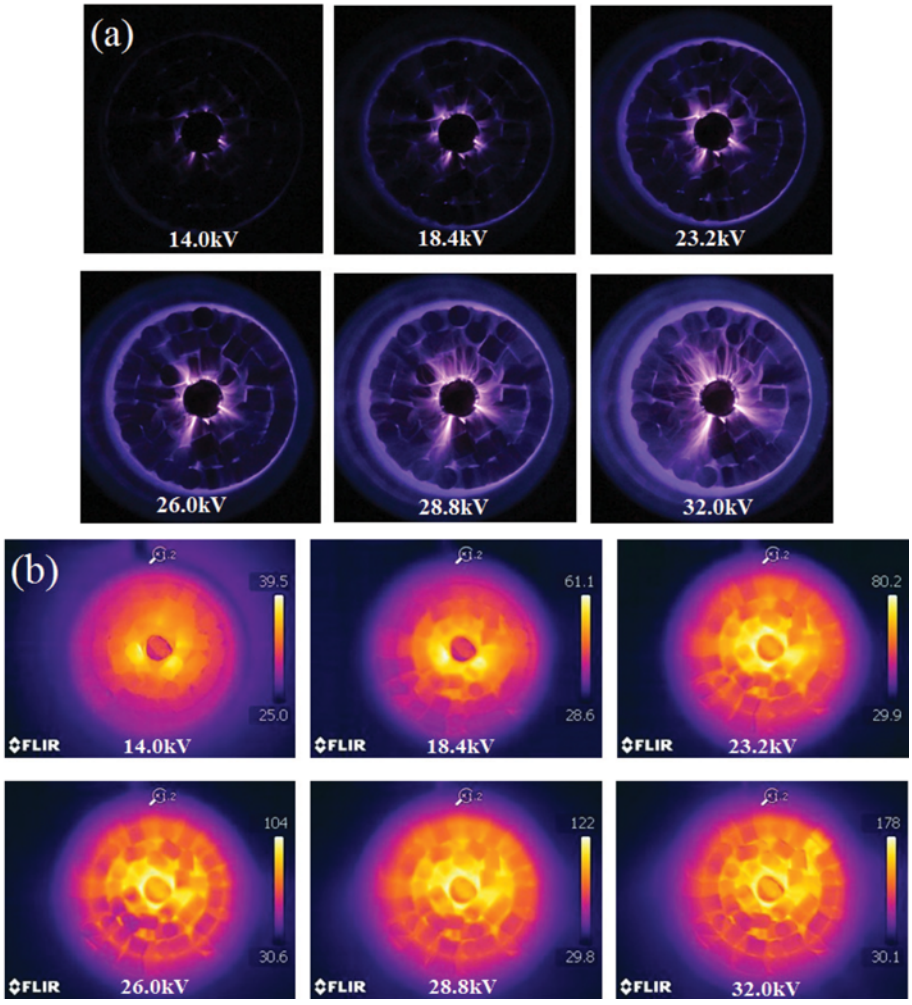


**Fig. 11. Optical (a) and IR (b) images of air plasma discharge in a γ-alumina packed-bed DBD reactor at different applied voltages.**

lar decomposition efficiency. It seems that butane decomposition efficiency is independent on the shape of the ZnO particles. The reason behind the similar decomposition efficiency despite the different shapes is that the primary decomposition of butane by plasma was sufficiently dominant such as to hide the photocatalytic effect. Even if the shape dependency of the butane decomposition efficiency itself was not significant, the distribution of byproducts was largely affected by the shape of ZnO. The desirable product of butane decomposition is definitely carbon oxides ($CO_x$). According to the FTIR spectra of the effluent, spherical ZnO NPs gave rise to several carbon-containing byproducts other than $CO_x$, such as acetaldehyde ($CH_3CHO$), propane ($C_3H_8$), and methane ($CH_4$), but this did not occur in the case of NWs and NRs. This result clearly indicates that the photocatalytic activity of ZnO depends on its particle shape. Furthermore, it is obvious that the selectivity towards $CO_x$ obtained with the ZnO NWs was higher than for the other shapes. The enhanced plasma-catalytic activity of ZnO NWs can be interpreted by the large surface to volume ratio, because ZnO NWs can provide large reactive boundaries that are available for reactions. The plasma-induced energy of UV illumination, however, was not confirmed in this work.

**5. Heat Effect**

Fig. 11 shows photos of the electrical discharge plasma at different applied voltages. The photos at the top were taken with an optical camera, whereas those at the bottom were recorded with an IR camera. At about 14 kV, the electrical discharge plasma was generated around the central electrode alone. As the voltage was further increased, the discharge gradually developed in the radial direction, and the entire region turned purple at about 32 kV. According to the infrared images, the hot zone radially propagated outward from the center as the voltage was increased. As mentioned above, the activation energy for plasma-catalysis can be provided by fast electrons, ozone, radicals, and local heating. These IR images demonstrate that local heating is also partially responsible for enhanced catalytic activity under plasma discharge.

## ENERGY-SAVING TECHNIQUES USING CYCLIC OPERATION

**1. Comparison between Continuous and Cyclic Operations for VOC Abatement**

A plasma-catalytic reactor can be operated in two modes, continuous and cyclic (see Fig. 12). The cyclic process differs from conventional continuous plasma treatment in that there are two steps to consider, adsorption and oxidation [62]. During adsorption, VOCs are enriched in the catalyst for several hours with the plasma turned off. In this manner, VOCs with a high flow rate and low concentration are converted to VOCs with a low flow rate and high concentration; this results in compact-sized control equipment and lower energy consumption [63]. Immediately after adsorption is complete, an air or oxygen plasma is turned on to catalytically oxidize the adsorbed VOCs to carbon dioxide and water vapor. Electrical energy is thus consumed only in this oxidation step. However, continuous operation consumes energy all the time; therefore, it is suitable for treating VOC-rich streams but not recommended for dilute VOC abatement in terms of energy efficiency.

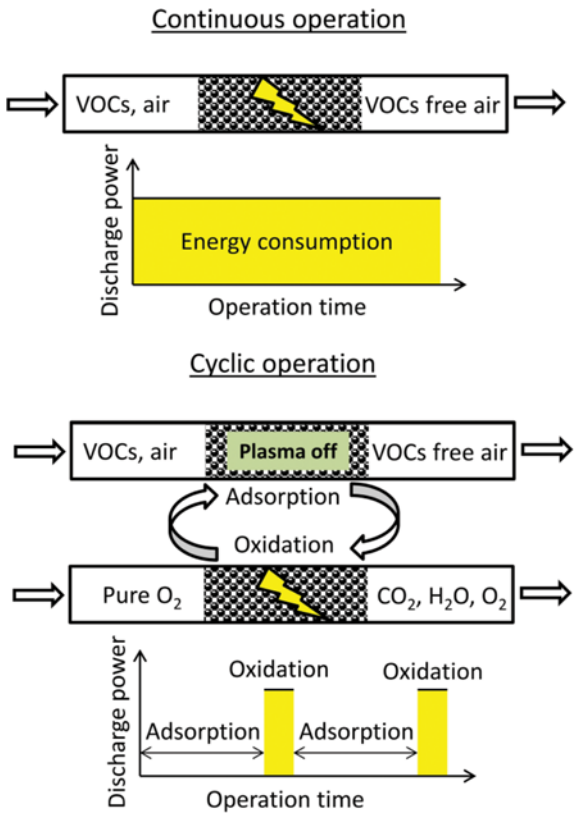


**Fig. 12. Continuous and cyclic operations in plasma-catalytic removal of VOCs.**

The required input energy generally decreases as the initial VOC concentration is lowered. However, for continuous plasma operation, even at very low VOC content, the input energy cannot be reduced below a certain value because the applied voltage should be significantly larger than the onset voltage to sustain uniform plasma generation. In most cases, a few hundreds of J $L^{-1}$ of SIE is required for continuous decomposition of VOCs. At this high input energy condition, the formation of nitrogen oxides is unavoidable, as their concentrations increase monotonically with injected power [64,65]. The formation of $NO_x$ limits the maximum applicable SIE to about 100 J $L^{-1}$ [66], eventually leading to plasma catalysis under continuous mode becoming less attractive from a practical viewpoint. As the cyclic treatment, which includes a long adsorption step followed by a short plasma oxidation step proceeds, the consumed energy is drastically reduced. In addition, the consumed energy decreases monotonically as the initial VOC concentration decreases, because the lower the VOC content, the longer the adsorption period. Besides, by using oxygen plasma, the regeneration of adsorbent is complete without $NO_x$ formation. As seen from Table 1, 56 J $L^{-1}$ is the injected energy needed to remove 90% of formaldehyde (2.2 ppm) from air by continuous plasma treatment [67]. However, at a formaldehyde concentration of 6.3 ppm, the cyclic operation is able to completely eliminate the VOC at an SIE of 7 J $L^{-1}$. The SIE can be further lowered to a few tenths of J $L^{-1}$ as the VOC concentration is of the order of parts per billion (ppb) - typical values in an indoor air environment [68]. According to the California Department of Public Heath (CDPH), the

**Table 1. Comparison of energy efficiency between continuous and cyclic treatment**

| VOC | Operation mode | Reactor type | Catalyst/Adsorbent | Concentration (ppm) | Flow rate (carrier gas) (L $min^{-1}$) | | SIE (J $L^{-1}$) | Removal efficiency (%) | Energy efficiency (g $kWh^{-1}$) | Ref. |
|---|---|---|---|---|---|---|---|---|---|---|
| | | | | | Ad. | De. | | | | |
| Toluene | (2) | Heating+ Surface discharge | HISIV-3000 and HISIV-1000 | 100 | 2.0 (air) | 0.5 (-) | 39[b] | >90 | 34.2 | [93] |
| | (1) | | | | - | | 679[b] | - | 1.97 | |
| | (2) | DBD One-stage | $\gamma$-$Al_2O_3$ | 500[b] (20.4 μmol $L^{-1}$) | 5.0 ($N_2$) | 2.5 ($O_2$) | 840[b] | 100[a] | 8.1[b] (41.2 J $μmol^{-1}$) | [71] |
| | (1) | DBD Two-stage | $CoMnO_x$/ZSM-5 | 107 | 1.0 (air) | | 330[a] | 93.7 | 4.22 | [94] |
| | | DBD One-stage | $FeO_x/Al_2O_3$/Ni foam | 108[b] (400 mg $m^{-3}$) | 0.45 (air) | | 140-320 | 45-100[a] | 1.37-1.24 | [52] |
| | | | $MnO_x/Al_2O_3$/Ni foam | | | | 140[b]-320[b] | 48.7-99.8 | 1.18-0.97 | [23] |
| Acetone | (2) | | Ag/$\beta$-zeolite | 300 | 2.0 ($N_2$) | 2.0 ($O_2$) | 126[b] | 97 | 19.72 | [70] |
| | (1) | | | | 2.0 (air) | | 840[b] | >99 | 3.05 | |
| | (1) | | $MnO_2/Al_2O_3$ monolith | | | | 120[a]- 1030[a] | 30-93 | 6.32[b]-2.30[b] | [48] |
| | | | $\gamma$-$Al_2O_3$ | 100 | 0.2 (air) | | 125[a]-635 | 25-80 | 3.70-2.30 | [29] |
| Formaldehyde | (2) | | AgCu/HZ | 6.3 | 0.3 (air) | 0.06 ($O_2$) | 7[b] | 100[a] | 4.0[b] ($1.9\times10^{-3}$ kWh $m^{-3}$) | [68] |
| | | | | ppb level | - | | - | - | $10^{-5}$-$10^{-4}$ kWh $m^{-3}$ | |
| | (1) | | Cu-Ce mixed oxide | 57.7 | 1.0 (air) | | 288-486 | 38[a]-94.7 | 0.3[b]-0.5[b] | [30] |
| | | DBD Two-stage | $MnO_x/gAl_2O_3$ | 2.2±0.1 | 6.0 (air) | | 2[a]-56[a] | 50[a]-90[a] | 3.1-0.2[a] | [67] |

(1) continuous operation, (2) cyclic operation
[a]Approximate values extracted from graphs
[b]Calculated from given data

VOC content of the air used to supply the conditioning environment, for example, should not exceed 5 μg $m^{-3}$ (equivalent to 4.1 ppb for formaldehyde) for any individual compound and 25 μg $m^{-3}$ for total volatile organic compounds (TVOC) [69]. From such a perspective, the sequential adsorptive capture and plasma-catalytic oxidation of VOCs are considered to be highly applicable to indoor air pollution control.

The energy efficiency defined by mass of VOC removed (g) per unit of electrical energy input (kWh) is used as a measure to evaluate the performance of a plasma process. In our previous study, the energy efficiency for the continuous plasma-catalytic removal of acetone (300 ppm) from an air stream (2.0 L $min^{-1}$) on Ag/$\beta$-zeolite was estimated to be ca. 3.05 g $kWh^{-1}$ [70]. Meanwhile, as the cyclic process was applied, the achieved performance was much higher, ca. 19.72 g $kWh^{-1}$. Similar results were also obtained for other typical VOCs such as toluene and formaldehyde, as shown in Table 1. The results in the table also indicate that for continuous operation, the energy efficiency is very poor at high SIE and thus at high VOC removal rate. However, the efficiency of the cyclic operation strongly depends on the adsorption capacity and catalytic activity of adsorbent/catalyst rather than on the input power because the higher the input power, the shorter the oxidation period [71].

Regarding byproduct formation, Xu et al. performed a direct comparison between continuous and cyclic operations for toluene decomposition on SBA-15 using gas chromatography-mass spectrometry (GC-MS) [72]. The intermediates deposited on the catalyst surface were extracted either after the continuous process reached its steady state or at different discharge times of cyclic treatment. Besides unreacted toluene, various partially oxidized species formed during the continuous decomposition of toluene were detected adsorbed on the catalyst surface. Among them, 4-methyl 2-nitrophenol, benzyl benzoate, benzyl alcohol and benzaldehyde were the most abundant (Fig. 13). Meanwhile, during cyclic treatment, only benzaldehyde and 2-heptene alcohol were found as adsorbed intermediates. These substances gradually accumulated on the catalyst surface within 45 min of discharge; however, they eventually disappeared at the end of the oxidation step, resulting in the regeneration of catalyst/adsorbent, higher toluene conversion, and carbon balance. The increased byproduct formation in the continuously fed system was attributed to homogeneous gas-phase reactions of toluene with reactive species as it reached the plasma region. According to Liang et al. [73], H-abstraction from the toluene methyl group by an OH radical results in the production of benzyl alcohol, which can be oxidized to benzaldehyde and subsequently to benzoic acid.

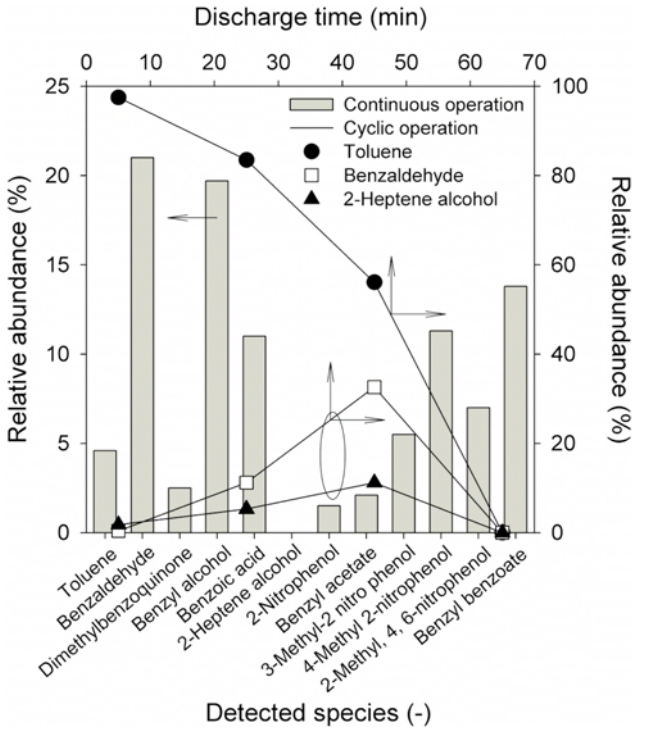


**Fig. 13. Intermediates on SBA-15 during toluene degradation at different discharge times of cyclic operation (air plasma, adsorption time: 72 min) and at a steady state of continuous operation under the same conditions (contaminated air flow rate: 0.1 L $min^{-1}$, initial toluene concentration: 21 ppm, and SIE: 317 J $L^{-1}$), data given in Ref. [72].**

**2. Reactor Configuration and Catalyst/Adsorbent for Cyclic Operation**

The investigation of cyclic operation mode is preferentially conducted with one-stage packed-bed reactors, because of the advantages resulting from direct plasma-catalyst interaction [74-76]. The authors tested the effects of the plasma reactor configuration on the oxidation of pre-adsorbed ethylene by pure air plasma [77]. Three reactors, including a one-stage partially packed-bed, a one-stage fully packed-bed, and a two-stage packed-bed (15 g of Ag exchanged 13X for each reactor), were used. For simplicity, these reactors were named the hybrid, one-stage, and two-stage reac-

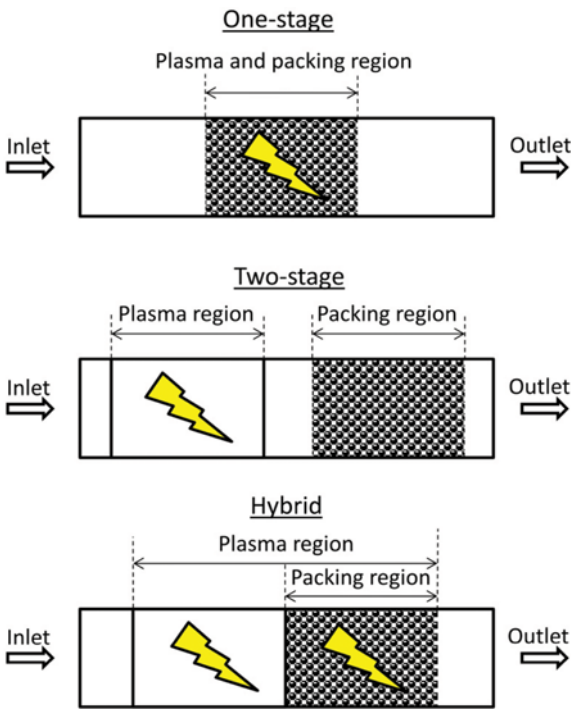


**Fig. 14. Packed-bed DBD reactor with different configurations.**

tors, respectively. The hybrid reactor comprised a sequential combination of two- and one-stage reactors, as shown in Fig. 14. The reactor performance was evaluated with respect to oxidation time and mineralization efficiency defined as the fraction of ethylene converted to carbon dioxide. Although the one- and two-stage reactors required more than 50 min for the complete oxidative desorption of ethylene (pre-adsorbed amount: 817.5 μmol for each reactor), the hybrid reactor almost regenerated the catalyst/adsorbent within only 20 min. Note that the discharge power of the hybrid reactor was only about twice as high as that of the former two reactor types, resulting in lower energy consumption. Based on the first 20 min plasma oxidation time, the mineralization efficiencies of the two-stage, one-stage, and hybrid reactors were estimated to be 10, 42, and 63%, respectively. These results show the positive effect of the effective utilization of both short-lived species, such as excited $N_2$, O atoms, and OH radicals in the plasma-catalyst phase, and long-lived species, especially ozone in the blank plasma gas phase for the oxidation of adsorbed VOCs.

For a single-bed multi-functional plasma reactor, the packing material can consist of either catalyst or adsorbent. Porous materials, such as zeolite [70], metal oxides (glass bead supported $TiO_2$ [78] and $Mn_xO_y$ [79]) and $\gamma$-alumina [71], are commonly used as catalyst/adsorbents for the plasma cyclic removal of VOCs. It is important to find an appropriate catalyst which possesses not only good plasma catalytic performance but also a large VOCs adsorption capacity [72]. The adsorption of VOCs on zeolite, for example, strongly relates to its Si/Al ratio, cation type, pore structure, and acidity as well as to the nature of the target VOCs [80,81]. For VOCs with a relatively low vapor pressure under normal conditions (e.g., toluene and acetone), the adsorption capacity is usually high on the parent zeolite [82]. However, for those highly volatile VOCs, such as ethylene, the modification of conventional adsorbents is often required. By loading silver onto 13X zeolite (30 g) using an ion exchange method, we observed that dilute ethylene (200 ppm) was completely removed from a gas stream (1.0 L $min^{-1}$) for a long period of about 260 min, corresponding to 2125.5 μmol of ethylene adsorbed [77], whereas the complete adsorption of the parent 13X required only 5 min under the same conditions. The enhanced adsorption capacity was attributed to the chemisorption of ethylene, resulting from the $\pi$-complexation of ethylene with silver. The high adsorption capability toward olefins on transition metal oxides was also obtained for the same reason [83-85]. Chemisorption, on the other hand, could lower the bond strength of adsorbed VOCs, facilitating VOC decomposition by reactive species.

Loading Ag nanoparticles onto zeolite not only enhances VOC adsorption, according to Kim et al. [86], it also assists discharge plasma to expand over a wide surface area, which is beneficial for the formation of chemically reactive species. In addition, the performance of a $TiO_2$-supported Ag catalyst for the oxidation of VOCs was greatly enhanced by increasing the oxygen content in plasma, making it a good choice over other metals such as Pt and Cu for cyclic systems [66]. For catalysts to be effective in a cyclic system, they require a positive $O_2$ partial pressure-dependence on both the decomposition efficiency and the $CO_2$ selectivity [87]. Our previous study showed that co-incorporation of Ag with other metals significantly affects the oxidative desorption of adsorbed ethylene [88]. Various catalyst/adsorbents (Ag/13X and Ag-$M_xO_y$/13X, M: Co, Cu, Mn, and Fe) have been used to investigate the influence of second metal oxides on the oxidation of pre-adsorbed ethylene. The high ozone killing activity of Ag-$MnO_x$/13X and Ag-$CoO_x$/13X suppressed the diffusion of ozone into zeolite micropores in which ethylene was captured, leading to poor mineralization. The good oxidation activity and the ability to allow a considerable amount of ozone to reach the inner surface enabled Ag-$Fe_xO_y$/13X to maintain a high $CO_2$ selectivity, while substantially reducing ozone emission. Nevertheless, Xu et al. reported the reverse effect of ozone decomposition activity for the cyclic plasma oxidation of toluene on AgMn/SBA-15 [72]. As mentioned above, the reactivity of target VOCs with ozone should be considered. Compared to toluene, the gas-phase reaction of ethylene with ozone is much faster ($k=1.06\times10^6$ and 234 $cm^3$ $mol^{-1}$ $s^{-1}$ at room temperature for ethylene and toluene, respectively) [89].

The reliability of the cyclic operation is also a matter of concern. The stability of the catalyst/adsorbent is assessed by continuously repeating sequential VOC adsorption and oxidation for several cycles. During the oxidation step, various species are formed that can strongly adsorb on the catalyst/adsorbent surface to compete for active sites with the target VOCs and plasma-induced active species. The accumulation of reaction products including water causes surface blockage and eventual deactivation of the catalyst/adsorbents. Choosing highly hydrophobic adsorbents such as $\beta$- and HZSM-5 zeolites (with high Si/Al ratio) can facilitate solving the issue of water adsorption. Our previous studies indicated that the obvious deactivation of the catalyst/adsorbents was not observed within four or five cycles of treatment [70,77]. The carbon oxides that were produced were similar for all oxidation steps, while VOCs were not detected at the outlet during adsorption. Although the long-term stability of catalyst/adsorbents should be further investigated, especially under conditions of humidity and co-existence of various VOCs, the experiments revealed plasma, in combination with catalysis/adsorption, to be highly capable of removing dilute VOCs from gas streams.

## REGENERATION OF DEACTIVATED CATALYST

When using the plasma-based process for the decomposition of VOCs, deactivation of the catalyst by the formation and deposition of non-volatile polymer-like compounds is an important issue for long-term stability, and the regeneration of the deactivated adsorbent should be reckoned with for practical applications.

Upon investigation, we found that the monolithic alumina supported $MnO_2$ catalyst was free from the deposition of polymer-like compounds [48]. This was investigated by infrared spectroscopy, for which the used $MnO_2$ catalyst was ground into a fine powder, after which the infrared spectrum was recorded. The infrared spectra of used and fresh $MnO_2$ catalysts were similar to each other, except for a trace of nitrate species observed at around 1,385 $cm^{-1}$ for the used catalyst (Fig. 15), indicating that the $MnO_2$ catalyst effectively prevents the formation of non-volatile polymer-like compounds due to its enhanced oxidation capability. In contrast, brownish non-volatile compounds accumulated on the inner

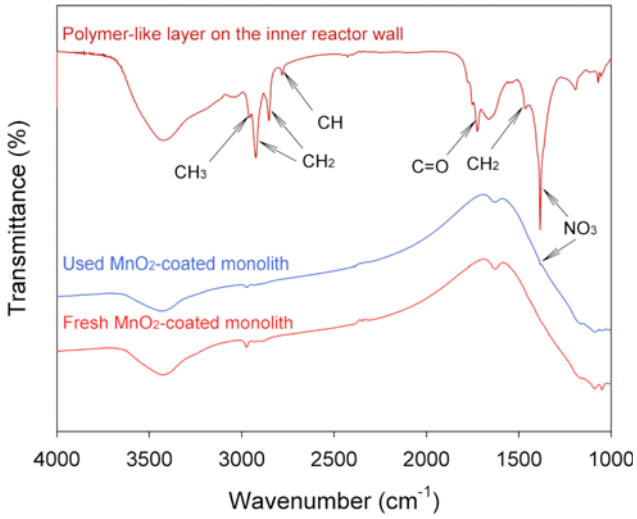


**Fig. 15. FTIR spectra of polymer-like layer on the inner wall and fresh and used $MnO_2$-coated monoliths.**

surface of the reactor wall in the absence of catalyst. Chen et al. [26] investigated the long-term stability of a catalytic SMF electrode coated with $TiO_2$ for the oxidation of toluene and found the reactor performance to be stable at ca. 90% of toluene conversion rate for 200 h (peak voltage: 40 kV, initial VOC concentration: 160 mg $m^{-3}$ and residence time: 4 s), whereas the conversion dropped from ca. 61% to ca. 54% for the bare SMF electrode under the same conditions. As a consequence, after the reaction, a brown oily deposit was observed on the bare electrode. Yet, the SMF+$TiO_2$ electrode was not observed to be covered with any polymerized materials. However, in other research, Subrahmanyam et al. [90] reported the deposition of nitrogen and carbon containing species on the $MnO_x$ catalytic electrode was revealed by XPS after the destruction of toluene, considered to be responsible for the degradation of catalytic activity. Thus, the degree of catalyst deactivation can depend upon the types of catalyst and reactor that were used, the target VOCs, as well as the applied conditions.

NTP has also been considered as promising for regenerating deactivated catalysts from other processes. The in-situ regeneration of deactivated Au/$TiO_2$ catalyst during CO oxidation using atmospheric NTP was intensively studied by Fan et al. [91]. The experiments revealed that pure oxygen plasma was able to fully restore the catalytic activity of Au/$TiO_2$ by oxidizing carbonate species deposited on the surface of gold nanoparticles. Nevertheless, $N_2$/$O_2$ plasma was unable to reversibly regenerate the catalyst, and even led to an additional poisoning effect due to the adsorption of NO, $NO_2$, and $N_2O_5$ formed in $N_2$/$O_2$ plasma. The strong deactivation of catalysts by adsorbed nitrogen oxides was also observed in our previous study of the ability of an air plasma to decompose residue ozone [45]. HafezKhiabani et al. [92] reported the investigation of the decoking of a Pt-Sn/$Al_2O_3$ catalyst in the naphtha reforming process using DBD and RF plasmas. Compared to conventional thermal regeneration methods, oxygen plasma is able to fully recover the catalytic activity without adverse effects on the internal structures of catalysts. The advantages of oxygen plasma in catalyst regeneration further support its capability to regenerate VOC-adsorbed adsorbents, as mentioned in the previous section.

## SUMMARY

Several mechanistic aspects that affect the overall performance of a plasma-catalysis system for the abatement of VOCs have been discussed. In the presence of a catalyst, surface reactions are promoted to be dominant, initially by the adsorption of reactants from the gas phase. Therefore, catalysts with larger surface areas are able to produce higher VOC removal rates. This is evidenced by the existence of O atoms or OH radicals on catalyst surfaces and their prolonged lifetime of as much as a few minutes on the time scale, thereby confirming the important role of catalysts in the utilization of plasma-induced reactive species, which are only able to survive in the gas phase for nanoseconds. The surface area, reducibility, and surface oxygen storage capacity are essential characteristics of a catalyst to govern the reaction performance. Under plasma activation, surface and even lattice oxygen can be activated for involvement in the oxidation of VOCs. Although the gas phase reactions of ozone with VOCs are usually slow, the reaction pathways can be altered in the presence of catalysts by regenerating atomic oxygen from the catalytic decomposition of ozone. The introduction of an ozone-destroying catalyst into plasma, however, does not always result in a positive effect on VOC decomposition. Neither an enhancement nor a negative effect is observed for some ozone-reactive VOCs. Thus, the nature of target VOCs should be considered when selecting an appropriate catalyst and reactor arrangement. Photocatalysis and local plasma-induced heating also contribute to overall reaction performance; however, their effects are evaluated to be minor in many cases.

With excellent performance in terms of energy and VOC decomposition efficiencies, $CO_2$ selectivity and free $NO_x$ formation, a cyclic operation using oxygen plasma is considered to be suitable in practice, especially for indoor air treatment. Future investigation should focus on seeking effective adsorbent/catalysts for the simultaneous removal of VOCs that typically coexist, as well as assessing the scale-up effects on reactor performance.

## ACKNOWLEDGEMENTS

This work was supported by the Basic Science Research Program through the National Research Foundation funded by the Ministry of Science, ICT and Future Planning, Korea (Grant No. 2013R1A2A2A01067961), and by the R&D Program of 'Plasma Advanced Technology for Agriculture and Food (Plasma Farming)' through the National Fusion Research Institute, Korea.

## NOTATION

$C_D$ : capacitance of dielectric [F]
$C_G$ : capacitance of gas gap [F]
$C_P$ : capacitance of packing material [F]
DE : decomposition efficiency [%]
L : active length of plasma reactor [m]
f : frequency of applied voltage [Hz]
P : average discharge power [W]

$R_P$ : radius of equivalent pellet layer [m]
$R_E$ : radius of inner electrode [m]
$R_D$ : outer radius of dielectric [m]
$R_{Di}$ : inner radius of dielectric [m]
$S_{BET}$ : specific surface area [$m^2\ g^{-1}$]
SIE : specific input energy [$J\ L^{-1}$]
$V_o$ : onset value of applied voltage [V]
$V_{peak}$ : peak value of applied voltage [V]

**Subscripts**

D : dielectric
G : gas gap
P : pellet or packing material
E : inner or HV electrode

**Greek Letters**

$\varepsilon_o$ : permittivity of free space, $8.854\times10^{-12}$ [$F\ m^{-1}$]
$\varepsilon_{rd}$ : relative permittivity of dielectric [F]
$\varepsilon_{rp}$ : relative permittivity of packing material [F]

## REFERENCES


1. S. Azalim, M. Franco, R. Brahmi, J. M. Giraudon and J. F. Lamonier, *J. Hazard. Mater.*, **188**(1-3), 422 (2011).
2. V. Nehra, A. Kumar and H. Dwivedi, *Int. J. Eng.*, **2**(1), 53 (2008).
3. T. Kuwahara, M. Okubo, T. Kuroki, H. Kametaka and T. Yamamoto, *Sensors*, **11**(6), 5529 (2011).
4. K. G. Kostov, R. Y. Honda, L. M. S. Alves and M. E. Kayama, *Braz. J. Phys.*, **39**(2), 322 (2009).
5. U. Kogelschatz, *Plasma Chem. Plasma Process.*, **23**(1), 1 (2003).
6. M. Chen, K. Takashima and A. Mizuno, *Int. J. Plasma Environ. Sci. Technol.*, **7**(1), 89 (2013).
7. Z. Abd Allah, J. C. Whitehead and P. Martin, *Environ. Sci. Technol.*, **48**(1), 558 (2014).
8. C. Ayrault, J. Barrault, N. Blin-Simiand, F. Jorand, S. Pasquiers, A. Rousseau and J. M. Tatibouët, *Catal. Today*, **89**(1-2), 75 (2004).
9. W. S. Kang, D. H. Lee, J. O. Lee, M. Hur and Y. H. Song, *Environ. Sci. Technol.*, **47**(19), 11358 (2013).
10. W. Liu, W. P. Addiego, C. M. Sorensen and T. Boger, *Ind. Eng. Chem. Res.*, **41**(13), 3131 (2002).
11. I. Biganzoli, R. Barni, A. Gurioli, R. Pertile and C. Riccardi, *J. Phys.: Conf. Ser.*, **550**, 012039 (2014).
12. L. Sivachandiran, J. Karuppiah and C. Subrahmanyam, *Int. J. Chem. React. Eng.*, **10**(1), 1542 (2012).
13. T. C. Manley, *J. Electrochem. Soc.*, **84**(1), 83 (1943).
14. A. Eid, K. Takashima and A. Mizuno, *IEEE Trans. Ind. Appl.*, **50**(6), 4221 (2014).
15. V. I. Parvulescu, M. Magureanu and P. Lukes, *Plasma chemistry and catalysis in gases and liquids*, Wiley-VCH, Weinheim (2012).
16. H. H. Kim, *Plasma Proc. Polym.*, **1**(2), 91 (2004).
17. S. Gourrier and M. Bacal, *Plasma Chem. Plasma Process.*, **1**(3), 217 (1981).
18. O. Guaitella, F. Thevenet, E. Puzenat, C. Guillard and A. Rousseau, *Appl. Catal., B*, **80**(3-4), 296 (2008).
19. K. V. Kozlov, H. E. Wagner, R. Brandenburg and P. Michel, *J. Phys. D: Appl. Phys.*, **34**(21), 3164 (2001).
20. O. Guaitella, C. Lazzaroni, D. Marinov and A. Rousseau, *Appl. Phys. Lett.*, **97**, 011502 (2010).
21. O. Guaitella, M. Hübner, S. Welzel, D. Marinov, J. Röpcke and A. Rousseau, *Plasma Sources Sci. Technol.*, **19**(4), 045026 (2010).
22. H. H. Kim, A. Ogata, M. Schiorlin, E. Marotta and C. Paradisi, *Catal. Lett.*, **141** (2), 277 (2011).
23. Y. Guo, X. Liao, J. He, W. Ou and D. Ye, *Catal. Today*, **153**(3-4), 176 (2010).
24. L. Sivachandiran, F. Thevenet, P. Gravejat and A. Rousseau, *Chem. Eng. J.*, **214**, 17 (2013).
25. X. Zhu, X. Gao, C. Zheng, Z. Wang, M. Ni and X. Tu, *RSC Adv.*, **4**, 37796 (2014).
26. J. Chen, Z. Xie, J. Tang, J. Zhou, X. Lu and H. Zhao, *Chem. Eng. J.*, **284**, 166 (2016).
27. Y. Guo, X. Liao and D. Ye, *J. Environ. Sci.*, **20**(12), 1429 (2008).
28. M. S. Gandhi, A. Ananth, Y. S. Mok, J. I. Song and K. H. Park, *Res. Chem. Intermed.*, **40**(4), 1483 (2014).
29. C. Zheng, X. Zhu, X. Gao, L. Liu, Q. Chang, Z. Luo and K. Cen, *J. Ind. Eng. Chem.*, **20**(5), 2761 (2014).
30. X. Zhu, X. Gao, R. Qin, Y. Zeng, R. Qu, C. Zheng and X. Tu, *Appl. Catal., B*, **170-171**, 293 (2015).
31. H. H. Kim, A. Ogata and S. Futamura, *J. Phys. D: Appl. Phys.*, **38**(8), 1292 (2005).
32. J. Jarrige and P. Vervisch, *Appl. Catal., B*, **90**(1-2), 74 (2009).
33. T. Zhu, Y. D. Wan, J. Li, X. W. He, D. Y. Xu, X. Q. Shu, W. J. Liang and Y. Q. Jin, *Int. J. Environ. Sci. Technol.*, **8**(3), 621 (2011).
34. A. M. Harling, D. J. Glover, J. C. Whitehead and K. Zhang, *Appl. Catal., B*, **90**(1-2), 157 (2009).
35. X. Tang, F. Feng, L. Ye, X. Zhang, Y. Huang, Z. Liu and K. Yan, *Catal. Today*, **211**, 39 (2013).
36. W. Li and S. T. Oyama, *J. Am. Chem. Soc.*, **120**(35), 9047 (1998).
37. M. T. N. Dinh, J. M. Giraudon, J. F. Lamonier, A. Vandenbroucke, N. D. Geyter, C. Leys and R. Morent, *Appl. Catal., B*, **147**, 904 (2014).
38. M. T. N. Dinh, J. M. Giraudon, A. M. Vandenbroucke, R. Morent, N. D. Geyter and J. F. Lamonier, *Appl. Catal., B*, **172-173**, 65 (2015).
39. Y. Li, Z. Fan, J. Shi, Z. Liu and W. Shangguan, *Chem. Eng. J.*, **241**, 251 (2014).
40. A. M. Vandenbroucke, M. Mora, C. J. Sanchidrián, F. J. R. Salguero, N. D. Geyter, C. Leys and R. Morent, *Appl. Catal., B*, **156-157**, 94 (2014).
41. S. Delagrange, L. Pinard and J. M. Tatibouet, *Appl. Catal., B*, **68**(3-4), 92 (2006).
42. Y. Li, Z. Fan, J. Shi, Z. Liu, J. Zhou and W. Shangguan, *Catal. Today*, **256**, 178 (2015).
43. A. M. Vandenbroucke, M. T. N. Dinh, N. Nuns, J. M. Giraudon, N. D. Geyter, C. Leys and R. Morent, *Chem. Eng. J.*, **283**, 668 (2016).
44. A. Ogata, K. Saito, H. H. Kim, M. Sugasawa, H. Aritani and H. Einaga, *Plasma Chem. Plasma Process.*, **30**(1), 33 (2010).
45. Q. H. Trinh and Y. S. Mok, *Catalysts*, **5**(2), 800 (2015).
46. J. O. Jo, S. B. Lee, D. L. Jang and Y. S. Mok, *IEEE Trans. Plasma Sci.*, **41**(10), 3021 (2013).
47. X. Zhu, X. Gao, X. Yu, C. Zheng and X. Tu, *Catal. Today*, **256**, 108 (2015).
48. H. Q. Trinh and Y. S. Mok, *Chem. Eng. J.*, **251**, 199 (2014).
49. R. Huang, M. Lu, P. Wang, Y. Chen, J. Wu, M. Fu, L. Chen and D.

Ye, *RSC Adv.*, **5**, 72113 (2015).
50. S. Yamamoto, S. Yao, S. Kodama, C. Mine and Y. Fujioka, *Open Catal. J.*, **1**(1), 11 (2008).
51. J. O. Jo, S. B. Lee, D. L. Jang, J. Park and Y. S. Mok, *Clean Technol.*, **20**(4), 375 (2014).
52. Y. Guo, X. Liao, M. Fu, H. Huang and D. Ye, *J. Environ. Sci.*, **28**, 187 (2015).
53. H. X. Ding, A. M. Zhu, F. G. Lu, Y. Xu, J. Zhang and X. F. Yang, *J. Phys. D: Appl. Phys.*, **39**(16), 3603 (2006).
54. S. Futamura, A. Zhang, H. Einaga and H. Kabashima, *Catal. Today*, **72**(3-4), 259 (2002).
55. M. Lu, R. Huang, J. Wu, M. Fu, L. Chen and D. Ye, *Catal. Today*, **242**, 274 (2015).
56. A. Ogata, H. H. Kim, S. M. Oh and S. Futamura, *Thin Solid Films*, **506-507**, 373 (2006).
57. S. Chavadej, K. Saktrakool, P. Rangsunvigit, L. L. Lobban and T. Sreethawong, *Chem. Eng. J.*, **132**(1-3), 345 (2007).
58. T. Sano, N. Negishi, E. Sakai and S. Matsuzawa, *J. Mol. Catal. A: Chem.*, **245**(1-2), 235 (2006).
59. K. Hashimoto, H. Irie and A. Fujishima, *Jpn. J. Appl. Phys.*, **44**(12), 8269 (2005).
60. S. Pekárek, J. Mikeš and J. Krýsa, *Appl. Catal., A*, **502**, 122 (2015).
61. M. S. Gandhi and Y. S. Mok, *Chemosphere*, **117**, 440 (2014).
62. K. Saulich and S. Müller, *J. Phys. D: Appl. Phys.*, **46**(4), 045201 (2013).
63. T. Kuroki, T. Fujioka, R. Kawabata, M. Okubo and T. Yamamoto, *IEEE Trans. Ind. Appl.*, **45**(1), 10 (2009).
64. A. Rousseau, A. Dantier, L. Gatilova, Y. Ionikh, J. Röpcke and Y. A. Tolmachev, *Plasma Sources Sci. Technol.*, **14**(1), 70 (2005).
65. H. H. Kim, A. Ogata and S. Futamura, *IEEE Trans. Plasma Sci.*, **34**(3), 984 (2006).
66. H. H. Kim, A. Ogata and S. Futamura, *Int. J. Plasma Environ. Sci. Technol.*, **1**(1), 46 (2007).
67. X. Fan, T. Zhu, Y. Sun and X. Yan, *J. Hazard. Mater.*, **196**, 380 (2011).
68. D. Z. Zhao, X. S. Li, C. Shi, H. Y. Fan and A. M. Zhu, *Chem. Eng. Sci.*, **66**(17), 3922 (2011).
69. California Department of Public Health, Emission testing method for California Specification 01350 (2010).
70. Q. H. Trinh, M. S. Gandhi and Y. S. Mok, *Jpn. J. Appl. Phys.*, **54**, 01AG04 (2015).
71. Y. S. Mok and D. H. Kim, *Curr. Appl. Phys.*, **11**(5), S58 (2011).
72. X. Xu, P. Wang, W. Xu, J. Wu, L. Chen, M. Fu and D. Ye, *Chem. Eng. J.*, **283**, 276 (2016).
73. W. J. Liang, L. Ma, H. Liu and J. Li, *Chemosphere*, **92**(10), 1390 (2013).
74. A. Ogata, K. Yamanouchi, K. Mizuno, S. Kushiyama and T. Yamamoto, *Plasma Chem. Plasma Process.*, **19**(3), 383 (1999).
75. H. X. Ding, A. M. Zhu, X. F. Yang, C. H. Li and Y. Xu, *J. Phys. D: Appl. Phys.*, **38**(23), 4160 (2005).
76. T. Kuroki, K. Hirai, R. Kawabata, M. Okubo and T. Yamamoto, *IEEE Trans. Ind. Appl.*, **46**(2), 672 (2010).
77. Q. H. Trinh and Y. S. Mok, *Catal. Today*, **256**, 170 (2015).
78. L. Sivachandiran, F. Thevenet and A. Rousseau, *Plasma Chem. Plasma Process.*, **33**(5), 855 (2013).
79. L. Sivachandiran, F. Thevenet and A. Rousseau, *Chem. Eng. J.*, **270**(15), 327 (2015).
80. K. J. Kim and H. G. Ahn, *Micropor. Mesopor. Mater.*, **152**, 78 (2012).
81. S. Sultana, A. M. Vandenbroucke, C. Leys, N. D. Geyter and R. Morent, *Catalysts*, **5**(2), 718 (2015).
82. Y. Teramoto, H. H. Kim, N. Negishi and A. Ogata, *Catalysts*, **5**(2), 838 (2015).
83. R. T. Yang and E. S. Kikkinides, *AIChE J.*, **41**(3), 509 (1995).
84. J. Padin and R. T. Yang, *Chem. Eng. Sci.*, **55**, 2607 (2000).
85. H. Kim, J. Park and Y. Jung, *Phys. Chem. Chem. Phys.*, **15**, 19644 (2013).
86. H. H. Kim, J. H. Kim and A. Ogata, *J. Phys. D: Appl. Phys.*, **42**(13), 135210 (2009).
87. H. H. Kim, A. Ogata and S. Futamura, *Appl. Catal., B*, **79**(4), 356 (2008).
88. Q. H. Trinh, S. B. Lee and Y. S. Mok, *J. Hazard. Mater.*, **285**, 525 (2015).
89. W. G. Mallard, F. Westley, J. T. Herron and R. Hampso, *NIST chemical kinetics database: Version 2Q98. Gaithersburg, MD*, USA: NIST (1998).
90. C. Subrahmanyam, A. Renken and L. K. Minsker, *Appl. Catal., B*, **65**(1-2), 157 (2006).
91. H. Y. Fan, C. Shi, X. S. Li, S. Zhang, J. L. Liu and A. M. Zhu, *Appl. Catal., B*, **119-120**, 49 (2012).
92. N. HafezKhiabani, S. Fathi, B. Shokri and S. I. Hosseini, *Appl. Catal., A*, **493**, 8 (2015).
93. T. Yamamoto, S. Asada, T. Iida and Y. Ehara, *IEEE Trans. Ind. Appl.*, **47**(5), 2235 (2011).
94. Y. Huang, S. Dai, F. Feng, X. Zhang, Z. Liu and K. Yan, *Environ. Sci. Pollut. Res.*, **22**(23), 19240 (2015).